InterPore JOURNAL

Supplementary Material

EVAPORATION IN THE PRESENCE OF PARTICLES IN A MODEL POROUS MEDIUM: IMPACT OF CORNER LIQUID FILMS

Elisa Ghiringhelli[1], Manuel Marcoux[1], Sandrine Geoffroy[2], Marc Prat[1]

[1]Institut de Mécanique des Fluides de Toulouse (IMFT), Université de Toulouse, CNRS – Toulouse, France; [2]LMDC (Laboratoire Matériaux et Durabilité des Constructions), Université de Toulouse, INSAT, UPS, France

APPENDIX A: IMAGING THE FINAL DEPOSIT

Images of the particle final deposit on the bottom wall of the channel network are obtained with the microscope equipped with a confocal green light and a 5x objective. The channel network is scanned after removal of the top glass and the underlying layer of PDMS.

The process for obtaining the deposit images follows these steps:

1. The opened micromodel is set under the microscope at the upper left corner. The green light is set at an intensity of 25% with the focus at the bottom of the channels.
2. The image frequency is set to 1s and the micromodel is manually scanned with a "snake by row" pattern, see **Figure 1a**.

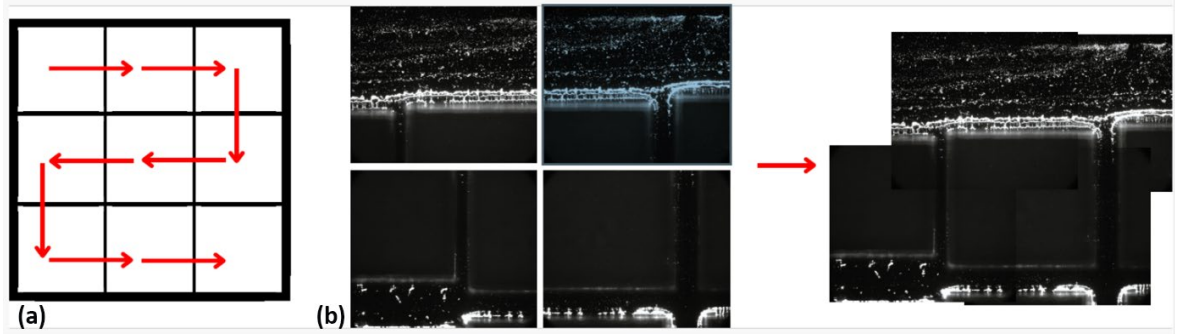

Figure 1: (a) Pattern used for scanning the deposit in the channels of the pore network. **(b)** Illustration of Fiji's plugin for stitching the images of the deposit. The particles correspond to the bright spots.

The next step consists in choosing the images in order to have an n × m matrix, noting that the dimensions can vary from one experiment to another since the scan is manual.

3. First, doubles and images not in focus are deleted.

At this point, the numbers of images for a row can vary from one row to the other. Then, m is the number of images in the row with the smallest number of images.

4. Images are deleted in order to get the same number m of images in every row.

5. As illustrated in **Figure 1b**, the images are then stitched together using Fiji's plugin "Stitching > Grid/Collection stitching" (https://imagej.net/software/fiji/downloads).
6. The fusion method is the linear blending method, where the intensities are smoothly adjusted between the images around the overlapping area.
7. After recombination of the images via the stitching procedure, an image of the particle deposit over the whole network is obtained as illustrated in **Figure 2**.

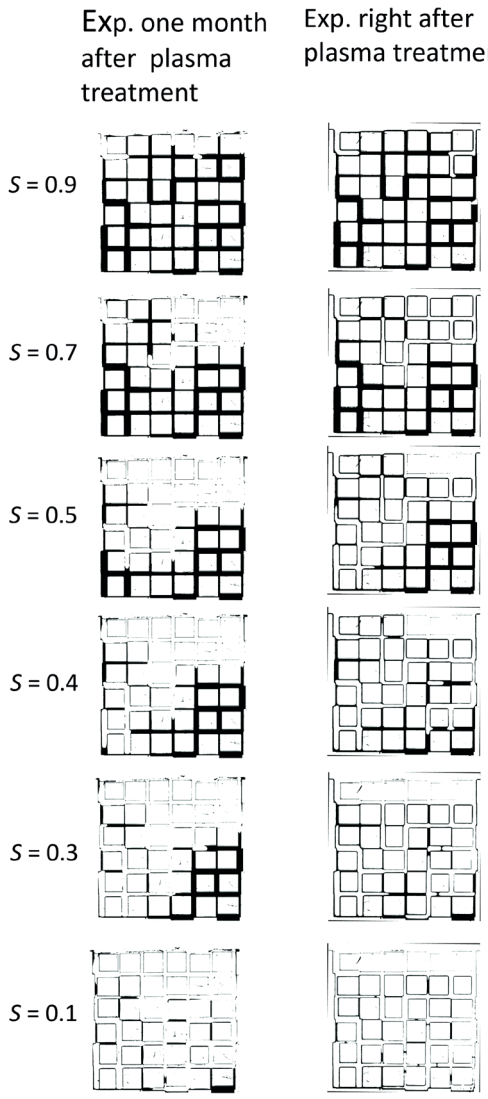

Figure 2: Comparison of drying patterns for liquid saturation S = 0.9, 0.7 and 0.5 (from left to right) for the experiments performed one month after the plasma treatment and the experiment performed right after the plasma treatment. The liquid phase is shown as black and the gas phase as white; vapor escapes through top edge of micromodel. The cell is held horizontally.

APPENDIX B: CORNER FILM MODEL

The notations are the same as the ones used in (4). Based on **Figure 3**, there are seven vertical lines of channels in the micromodel connecting the reservoir to the opposite closed end of micromodel (bottom edge in **Fig. 3**). Therefore, the micromodel is represented by a system of seven straight channels in parallel. Therefore, the evaporation rate from one channel can be estimated as $J_{ch} = jA/7$, where j is the evaporation flux and A is the micromodel cross-section surface area ($A = Wa$, where W is the micromodel width (1.8 cm, **Fig. 3a**) and a is the channel depth (a = 1mm). As in **Appendix B**, computations are made for the evaporation flux $j = 10^{-4}$ kg/m^2/s. The channels are of uniform rectangular cross-section. The length L of the channels is equal to the length of the micromodel, i.e. $L = 1.9$ cm (**Fig. 3a**). Consistently with the micromodel channel characteristics, we consider channel rectangular cross sections of width in the range [80 µm - 910 µm] and depth of 1 mm. As in (2), we assume that corner films only develop along the SUEX corners and not along the PDMS/SUEX corners. This can be questioned since the contact angle on PDMS can be lower than 45° right after the plasma treatment (1) but is a conservative assumption since the flow rate in one corner film is greater when only two corner films per channel are considered. Thus, we consider that two corner films are present in a channel.

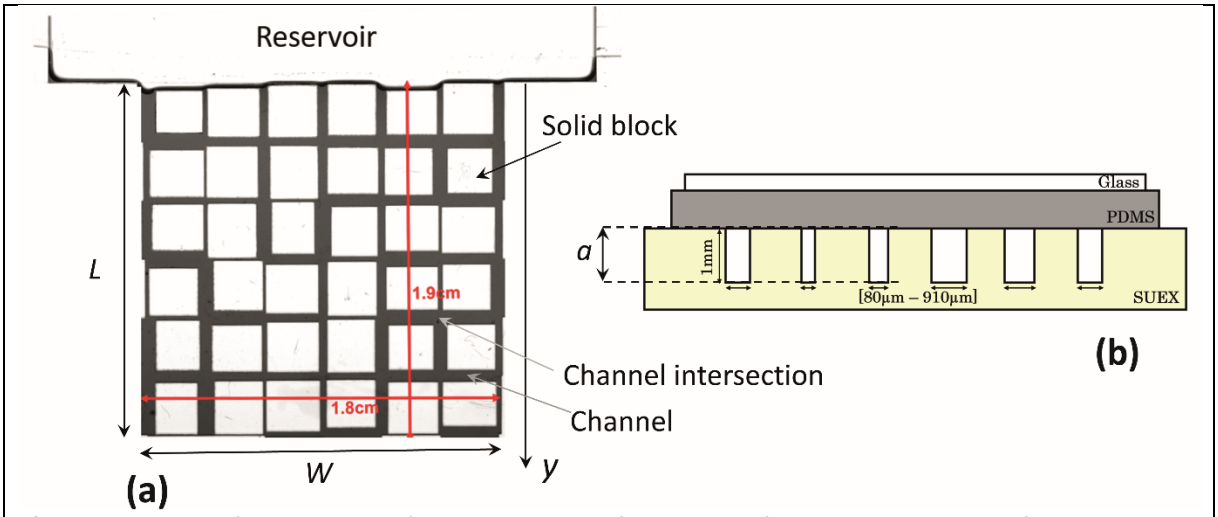

Figure 3: (a) Top view of composite SUEX-PDMS micromodel with square network of interconnected channels of the rectangular cross section. The image is with liquid (in black) in the channels. **(b)** Sketch of a cross section of the micromodel with the various layers; the PDMS is colored grey for illustration, but in reality, it is transparent.

The flow rate within a corner film is expressed as in (4). In the case of a channel with two corner films, the corner film flow rate in the channel reads as shown in **Equation 1** below, where $y = 0$ is at the entrance of micromodel (micromodel-reservoir interface in **Fig. 3a**) and $y = L$ corresponds to the opposite edge of micromodel (bottom edge in **Fig. 3a**).

$$q_m = -2\rho_\ell \frac{A_c R^2}{\beta\mu}\frac{dp}{dy} \qquad 0 \le y \le L \qquad (1)$$

In **Equation 1**, R is the corner film curvature radius, p is the pressure in the liquid, μ is the liquid dynamic viscosity, A_c is the corner film cross section surface area in the channel and β is a dimensionless resistance. The latter can be expressed for a sharp corner as (4), as shown in **Equation 2**, on the next page.

$$\beta = \frac{12(\sin\alpha)^2(1-B)^2}{(1-\sin\alpha)^2 B^2}\frac{{\psi_3}^2}{(\psi_1 - B\psi_2)^2} \qquad (2)$$

where we then have the following equations:

$$\psi_1 = (\cos(\alpha+\theta))^2 + \cos(\alpha+\theta)\sin(\alpha+\theta)\tan\alpha \quad (3)$$

$$\psi_2 = 1 - \frac{\theta}{\frac{\pi}{2}-\alpha} \quad (4)$$

$$\psi_3 = \frac{\cos(\alpha+\theta)}{\cos\alpha} \quad (5)$$

and $B = \left(\frac{\pi}{2}-\alpha\right)\tan\alpha$, in which θ is the contact angle expressed in radian and $\alpha = \frac{\pi}{4}$. The corner film cross section surface area for two corner films can be expressed as **Equation 6** where $\psi_4 = \frac{cos\theta}{sin\alpha}\cos(\alpha+\theta) - \frac{\pi}{2} + \alpha + \theta$.

$$A_c = 2R^2\psi_4 \quad (6)$$

The pressure in the liquid is linked to the surface tension and *R* by the Young-Laplace law, as shown in **Equation 7** where p_g is the gas pressure assumed constant.

$$p = p_g - \frac{\gamma}{R} \quad (7)$$

The above equations are combined to obtain **Equation 8** where $\kappa = \psi_4/\beta$.

$$q_m = \frac{2\rho_\ell \kappa\gamma R^2}{\mu}\frac{dR}{dy} \quad (8)$$

The flow is induced by the evaporation at the film tip (at $y = 0$) rate. Thus, we have **Equation 9** where J_{ch} is the evaporation rate from one channel.

$$\frac{2\rho_\ell \kappa\gamma R^2}{\mu}\frac{dR}{dy} = J_{ch} \quad (9)$$

Equation 9 is used to solve with the boundary condition $R = R_{th}$ at $y = L$, where R_{th} is the corner film curvature radius near the micromodel bottom edge (at $y = L$). It is considered here that a main meniscus is present at $y = L$. Thus, R_{th} is the corner film curvature radius at the junction between the corner films and the main meniscus. The solution to **Equation 9** reads as follows in **Equation 10**:

$$R^3 = \frac{3J_{ch}\mu}{2\rho_\ell \kappa\gamma}(y-L) + R_{th}^3 \quad (10)$$

The curvature radius R_{th} is determined by expressing the continuity of the capillary pressure between the main meniscus and the corner films, namely **Equation 11**, where we have assumed a contact angle of 90° on PDMS for simplicity:

$$\frac{\gamma}{R_{th}} = \gamma\left(\frac{2cos\theta_{SUEX}}{w} + \frac{cos\theta_{SUEX}}{a}\right) \quad (11)$$

The expression of the main meniscus capillary pressure in Equation 11 (right hand side of the equation) is an approximation judged sufficient for the present work (see (3) for a more refined approach).

According to **Equation 10**, the maximum length of corner films is given by **Equation 12**:

$$L_{film-max} = R_{th}^3 \frac{2\rho_\ell \kappa \gamma}{3J_{ch}\mu} \tag{12}$$

Using **Equation 12** leads to the results presented in **Figure 4** below.

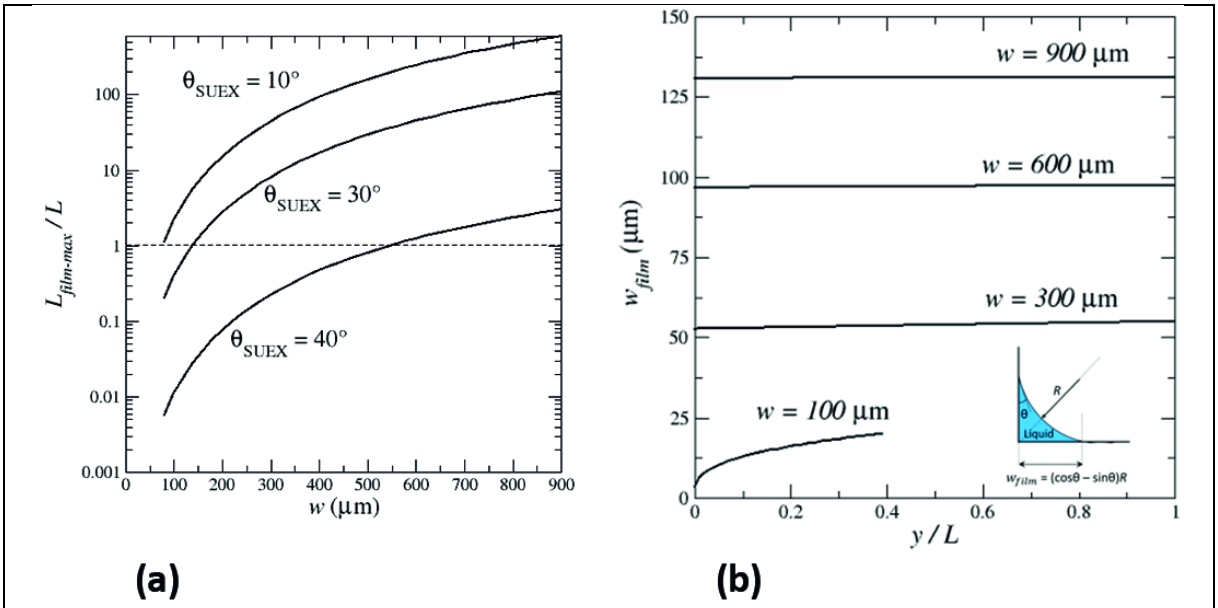

Figure 4: a) Maximum length of corner films resulting from the competition between viscosity and capillarity effects as a function of channel width for the three contact angle values. **(b)** The variation of corner film thickness over the micromodel length for the various channel widths when θ = 30°. When w = 100 μm, the film thickness distribution is shown when the corner films are about to recede into the channel.

APPENDIX C: PATTERNS - COMPARISON WITH PURE WATER EXPERIMENT

Figure 5 is a comparison of the drying patterns for the liquid saturation of S = 0.9, 0.7, and 0.5, for the experiments performed one month after the plasma treatment and the experiment performed right after the plasma treatment. The liquid phase is shown as black and the gas phase as white; vapor escapes through top edge of micromodel. The cell is in horizontal arrangement.

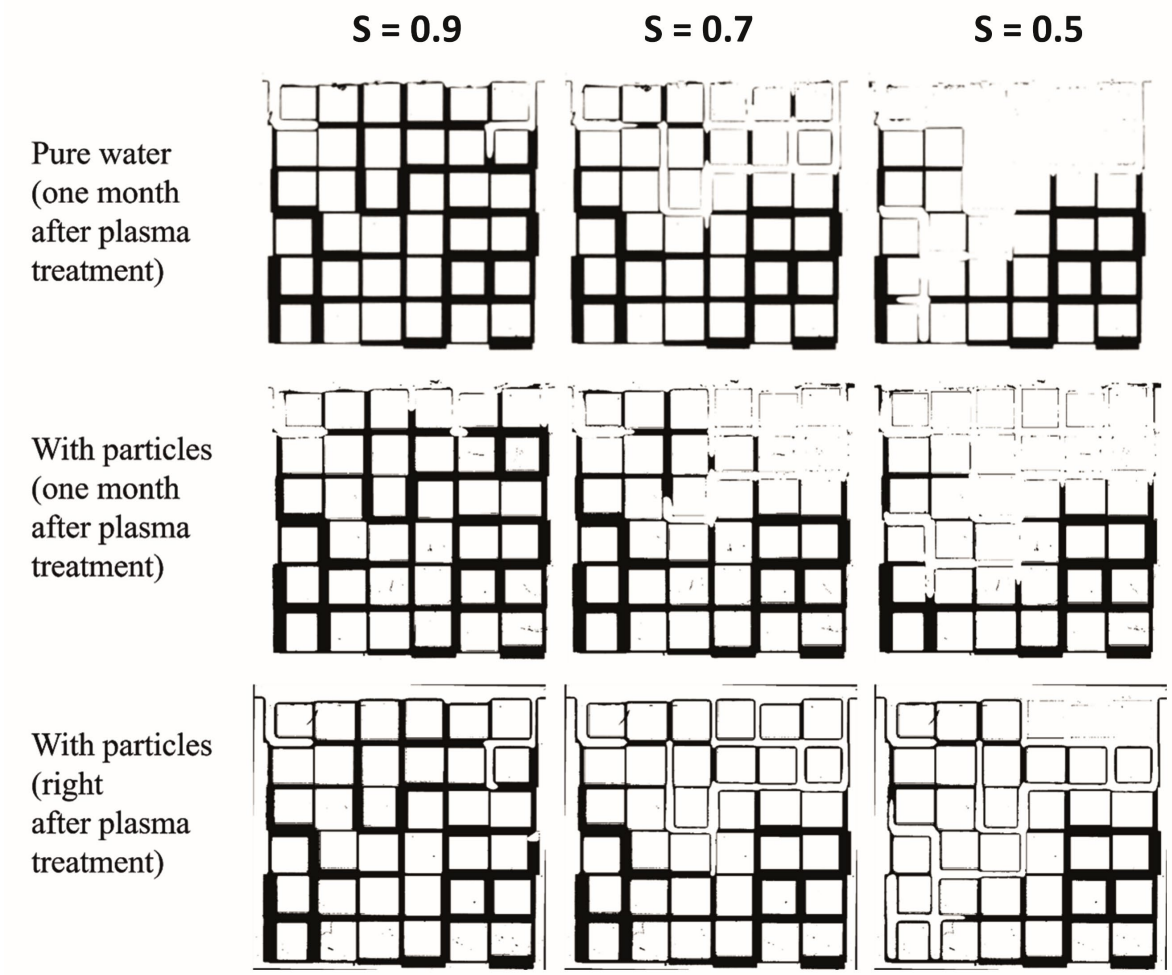

Figure 5: Drying patterns for the liquid saturation of S = 0.9, 0.7, and 0.5 at three different time points.

APPENDIX D: PÉCLET NUMBER EVALUATION

The Péclet number is defined as shown in **Equation 13**, where j is the evaporation flux (kg/m^2/s), ρ_ℓ is the liquid density (j / ρ_ℓ is an evaporation characteristic velocity), H is the micromodel height (1.9 cm), ε is the porosity (~0.5), D_{eff} is the micromodel effective diffusion coefficient of the particles (5).

$$Pe = \frac{jH}{\rho_\ell \varepsilon D_{eff}} \tag{13}$$

For a square network, $D_{eff} \sim D_p$ (weak tortuosity) where D_p is the particle diffusion coefficient. The latter is estimated from the Einstein-Stokes law as **Equation 14** where k = 1,380 649 × 10^{-23} J K^{-1} is the Boltzmann constant, d_p is the particle diameter and μ is the dynamic viscosity.

$$D_p = \frac{kT}{6\pi\mu\,(\frac{d_p}{2})} \tag{14}$$

For our particles (d_p = 1 µm) and water μ = 1 × 10^{-3} Pa, one obtains $D_p \approx$ 4.3 x 10^{-13} m^2/s. An estimate of j can be obtained from **Figure 6** noting that 80% of the initial mass of liquid (0.14 g) has evaporated in about 1000 min. This gives $j \sim$ 10^{-4} kg/m^2/s and $Pe \sim 9000$. This value was computed with the evaporation flux corresponding to the pure water experiment in **Figure 6**. The conclusion is therefore that the Péclet is very high in the experiment.

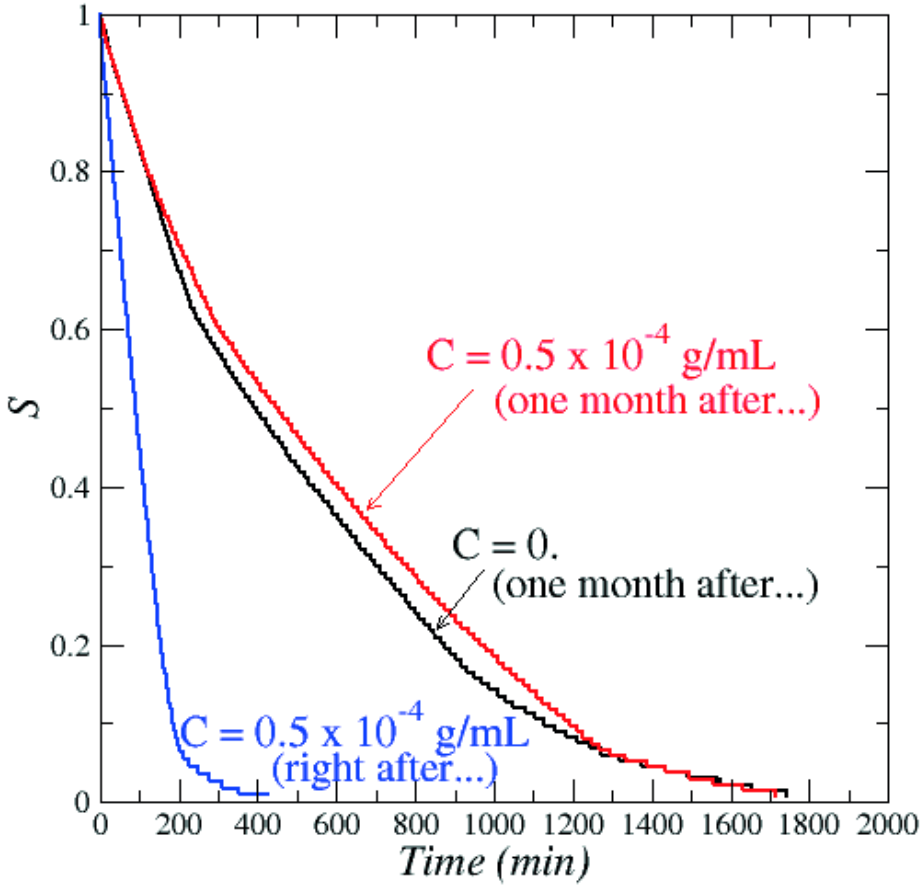

Figure 6: Variations of the overall liquid saturation as a function of time for the experiments being performed one month after the plasma treatment versus right after the plasma treatment.

REFERENCES

1. Bodas, D. & Khan-Malek, C (2006). Formation of more stable hydrophilic surfaces of PDMS by plasma and chemical treatments. *Microelectronic Engineering,* 83, 1277–1279. https://doi.org/10.1016/j.mee.2006.01.195
2. Ghiringhelli, E., Marcoux, M., Geoffroy, S., & Prat, M. (2023). Evaporation in a single channel in the presence of particles. *Colloids and Surfaces A: Physicochemical and Engineering Aspects*, 656, 130432. https://doi.org/10.1016/j.colsurfa.2022.130432
3. Mason, G., & Morrow, N. R. (1984). Meniscus curvatures in capillaries of uniform cross-section. *Journal of the Chemical Society, Faraday Transactions 1: Physical Chemistry in Condensed Phases*, 80(9), 2375. https://doi.org/10.1039/f19848002375
4. Prat, M. (2007). On the influence of pore shape, contact angle and film flows on drying of capillary porous media. *International Journal of Heat and Mass Transfer*, 50(7–8), 1455–1468. https://doi.org/10.1016/j.ijheatmasstransfer.2006.09.001
5. Whitaker, S. (1999). *The method of volume averaging* (Vol. 13). Springer Netherlands. https://doi.org/10.1007/978-94-017-3389-2